

From Inpainting to Layer Decomposition: Repurposing Generative Inpainting Models for Image Layer Decomposition

Jingxi Chen¹, Yixiao Zhang², Xiaoye Qian², Zongxia Li¹,

Cornelia Fermuller¹, Caren Chen², Yiannis Aloimonos¹

¹University of Maryland

²Amazon

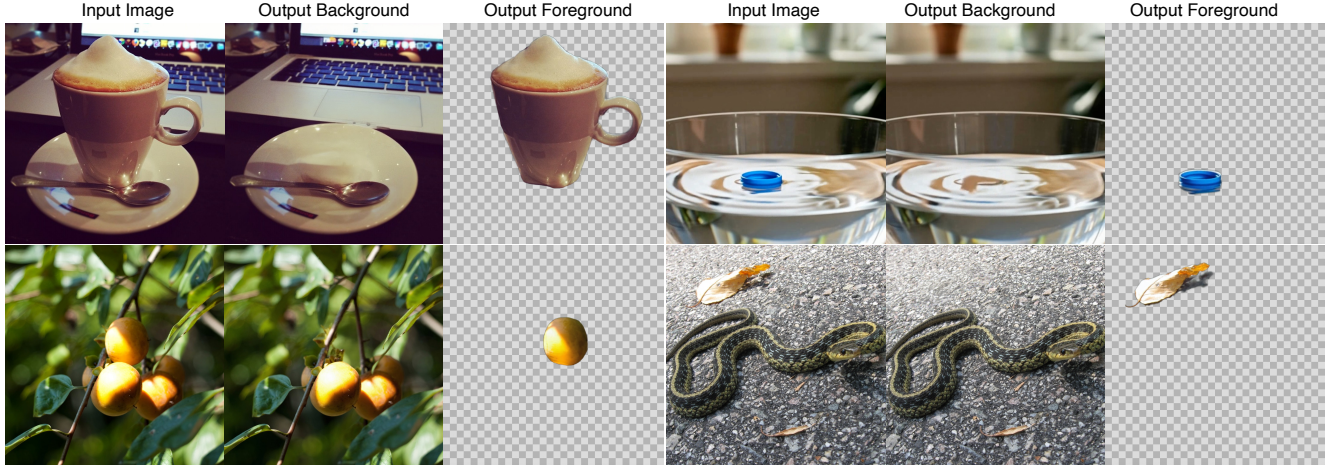


Figure 1. We propose a novel method for image layer decomposition, that is able to simultaneously extract foreground object with potential occlusion recovered, and remove the object from the background. The model is efficiently adapted from a pre-trained inpainting model. For each set of images in this figure, left is the original image, middle is the background and right is the foreground.

Abstract

Images can be viewed as layered compositions, foreground objects over background, with potential occlusions. This layered representation enables independent editing of elements, offering greater flexibility for content creation. Despite the progress in large generative models, decomposing a single image into layers remains challenging due to limited methods and data. We observe a strong connection between layer decomposition and in/outpainting tasks, and propose adapting a diffusion-based inpainting model for layer decomposition using lightweight finetuning. To further preserve detail in the latent space, we introduce a novel multi-modal context fusion module with linear attention complexity. Our model is trained purely on a synthetic dataset constructed from open-source assets and achieves superior performance in object removal and occlusion recovery, unlocking new possibilities in downstream editing and creative applications.

1. Introduction

Recent advances in generative modeling, particularly diffusion models, have greatly improved image synthesis and manipulation. While most image diffusion models [18, 22, 27] target single tasks like inpainting, super-resolution, or image translation, they excel at generating plausible content in under-constrained scenarios. However, real-world applications often require a combination of related tasks. One such task is image layer decomposition, simultaneously extracting the foreground and completing the background, which goes beyond inpainting and supports applications like creative re-composition, layered artwork generation, and component-based retrieval.

While single-task image diffusion models have been widely studied, diffusion-based image layer decomposition remains underexplored. A recent work [30] addresses this by fully fine-tuning a closed-source, pre-trained text-to-image model on a large, curated dataset. Although effective, this approach demands substantial computational resources and data. In contrast, we observe that decomposed backgrounds

involve filling masked regions, while foregrounds extend unmasked regions with an additional alpha channel. This conceptual similarity to inpainting and outpainting motivates our approach: to achieve layer decomposition through efficient adaptation of a pre-trained model, without large-scale training.

The central research question of this work is: *What is the relationship between image layer decomposition and inpainting, and can existing inpainting models be effectively adapted to perform layer decomposition?*

This question drives our investigation into whether lightweight repurposing of inpainting models can offer a practical alternative to large-scale retraining for image layer decomposition. This direction is valuable to both researchers and practitioners, as training generative models from scratch is increasingly costly in terms of compute and data. In contrast, numerous pre-trained models already exist for standard tasks like inpainting. If these models can be effectively adapted for layer decomposition with minimal effort, it would significantly reduce development overhead and enable a plug-and-play extension that benefits from future advances in inpainting models.

In this work, we introduce the first approach to adapt a pre-trained image inpainting model for the novel task of image layer decomposition, as illustrated in Figure 1. By examining the fundamental relationship between inpainting and layer decomposition, we observe that the latter extends inpainting by requiring not only background completion but also foreground extraction and outpainting. This insight motivates our method, *Outpaint-and-Remove*, which efficiently adapts a pre-trained diffusion-based inpainting model to perform image layer decomposition in a parameter- and data-efficient manner.

For robust evaluation, we conduct experiments on the MULAN [25] dataset, which is the only standard dataset in this domain to the best of our knowledge. We also conduct user study on a small set of real-word high quality images. Both qualitative and quantitative results show state-of-the-art performance on the novel task of image layer decomposition, as well as on standard object removal. Our ablation studies further validate the effectiveness of our design, demonstrating that augmenting a pre-trained inpainting model significantly improves its ability to perform layer decomposition. Our main contributions are summarized as follows:

- A novel perspective of layer decomposition, and a light-weight adaptation method that enables pre-trained image inpainting diffusion models to perform layer decomposition efficiently.
- Comprehensive experiments and ablations demonstrate that our adaptation-based approach effectively leverages publicly available models and datasets to achieve state-of-the-art performance on both image layer decomposition and the original inpainting task.

2. Related Work

2.1. Image Diffusion Models

Diffusion models (or related flow-based models) have dominated image generation since the pioneering work DDPM [9], outperforming VAE-based [13] and GAN-based [7] approaches in diversity, robustness, and scalability. While alternatives such as autoregressive models [24] have been proposed, most state-of-the-art text-to-image models remain within the diffusion paradigm [2, 21]. Diffusion models have also been successfully adapted to a wide range of image tasks, including inpainting [4, 18, 29], super-resolution [6], image translation [2, 15], and even discriminative tasks like segmentation and matting [1, 10].

2.2. Image inpainting Models

Early image inpainting methods typically rely on training convolutional neural networks or transformers from scratch on curated datasets [23, 32, 33]. More recently, diffusion-based generative models have become the dominant approach for inpainting, driven by both industrial [5, 16] and open-source [12] efforts. Compared to traditional methods, these models offer greater diversity through sampling and better controllability via prompt conditioning.

2.3. Image Layer Decomposition

Layer decomposition enables flexible element-wise image editing that is infeasible with single-layer images. However, high-quality layer-annotated datasets remain scarce in the open-source community. MULAN [25] provides a large-scale dataset with RGBA layers, but these are generated using off-the-shelf detection, segmentation, or inpainting models, and their quality is not guaranteed. LayerDiffuse [34] and Alfie [20] repurpose diffusion models to synthesize RGBA layers. In our work, we leverage MULAN and LayerDiffuse as foreground layer data sources. LAYERDECOMP [30] is a recent method explicitly targeting the layer decomposition task. The key distinction between LAYERDECOMP and our approach lies in training philosophy: LAYERDECOMP fully fine-tunes a Diffusion Transformer (DiT) on a close-sourced large-scale dataset, whereas we reveal the close relationship between inpainting and layer decomposition, and show that the latter can be achieved via lightweight fine-tuning on a pre-trained inpainting model, requiring significantly less data and computational cost.

3. Proposed Approach

3.1. Problem Formulation

The core idea of our method is that image layer decomposition can be reformulated as a combination of inpainting and outpainting tasks. Rather than designing a model from

scratch, we show that a single inpainting model can be efficiently fine-tuned to handle this task.

In this section, we discuss the conceptual connection between image inpainting and layer decomposition, and explain how we adapt the inpainting formulation to simultaneously recover missing regions (inpainting) and extend visible content beyond its original boundaries (outpainting), effectively enabling layered decomposition.

Image inpainting: The image inpainting problem can be formulated as follows: given an input image I and a binary mask M , a diffusion-based inpainting model f_{θ_1} takes the masked image $I \cdot M$ as input and predicts the missing content in the region indicated by M . Here, \cdot denotes the element-wise masking operation that removes the target region in I for the purpose of inpainting.

Image Layer Decomposition: For the Image Layer Decomposition, given an input image I and a binary mask M , a diffusion-based model f_{θ_2} takes the image I and M as input and outputs both the extracted foreground indicated by M , which may include occluded regions, and a completed background with the foreground object removed. The key difference from image inpainting lies not only in the additional foreground output but also in the treatment of the background. As shown in Figure 6, an inpainting model simply fills the masked region with plausible content, while layer decomposition requires explicit object removal, restoring the background as if the object never existed.

Nevertheless, we observe a structural unification between inpainting and layer decomposition tasks. For the background layer, both approaches involve filling masked regions with plausible content. For the foreground layer, the goal is to recover accurate RGB and alpha channels within the masked object, while enforcing zero alpha outside, effectively an outpainting formulation with transparency constraints. This dual formulation allows both foreground and background generation to be viewed as special cases of in/out-painting. As modern diffusion models are generalists due to large-scale pre-training, we propose reusing a single inpainting backbone with minimal modifications, adding a lightweight foreground prediction head, to support image layer decomposition via parameter-efficient fine-tuning.

3.2. Pipeline Overview

We present an overview of our proposed Outpaint-and-Remove pipeline in Figure 2. In the Figure 3, We detail our proposed method and key components. We also explain our unique data curation strategy built entirely from open-source datasets and tools in Figure 5.

3.3. Multi-Modal Context Tokenization

Modern diffusion or flow models work on tokens in a latent space. To preserve as much fine details as possible in the latent space, we are motivated to exploit multi-modal

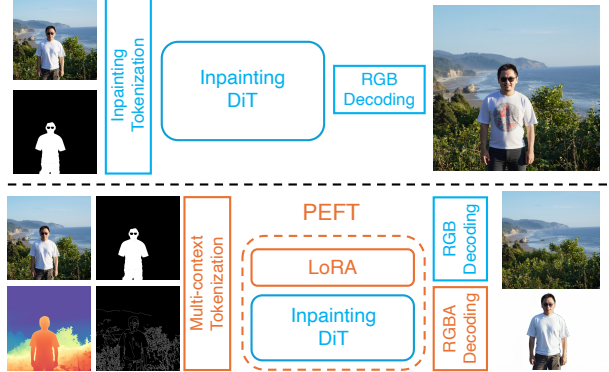


Figure 2. The top illustrates the original inpainting functionality of the pre-trained Inpainting DiT. The bottom shows our adapted pipeline for the image layer decomposition task. We introduce three key components to the pre-trained model for the adaptation: 1) Multi-Modal context Tokenization, 2) Parameter-Efficient Fine-Tuning (PEFT), 3) RGBA Decoding. Original components from the pre-trained model are highlighted in light blue, while our added or modified components are shown in orange.

context inputs as conditions for generation. Specifically, we produce the edge map, segmentation map and depth map from the given image. Given the image, mask, and multi-modal maps obtained, we first convert all these image-like inputs into tokens. With recent advances in VAE encoders from pre-trained DiT models, we find these encoders can effectively tokenize various image-like inputs, as verified in our supplementary material.

However, when we want to incorporate more modalities context tokens as additional inputs, challenge arises from the computational overhead introduced by the growing number of tokens. To address this, we propose summarizing the multi-modal tokens into a compact representation before feeding them into the DiT. While token fusion is best handled by a transformer-like module, standard attention has quadratic complexity, $O(K^2)$, where K is the total number of tokens from all modalities. To reduce this cost, our proposed Multi-Modal Latent Fusion module, inspired by linear attention transformers [11, 19], uses a small constant number $N \ll K$ of latent tokens as queries. This reduces the attention complexity to approximately $O(KN)$, making it linear with respect to the number of input tokens.

3.4. Design of the Image-Mask Context

The design of the image-mask context plays a critical role in our method. As shown in the ablation study (Section 4.4.2), the choice of image-mask context directly reflects the nature of the task, a combination of foreground outpainting and background removal.

Our context design is illustrated in Figure 4. Unlike standard diffusion-based inpainting models that use only a background image-mask context c_{I-M}^b , we introduce an

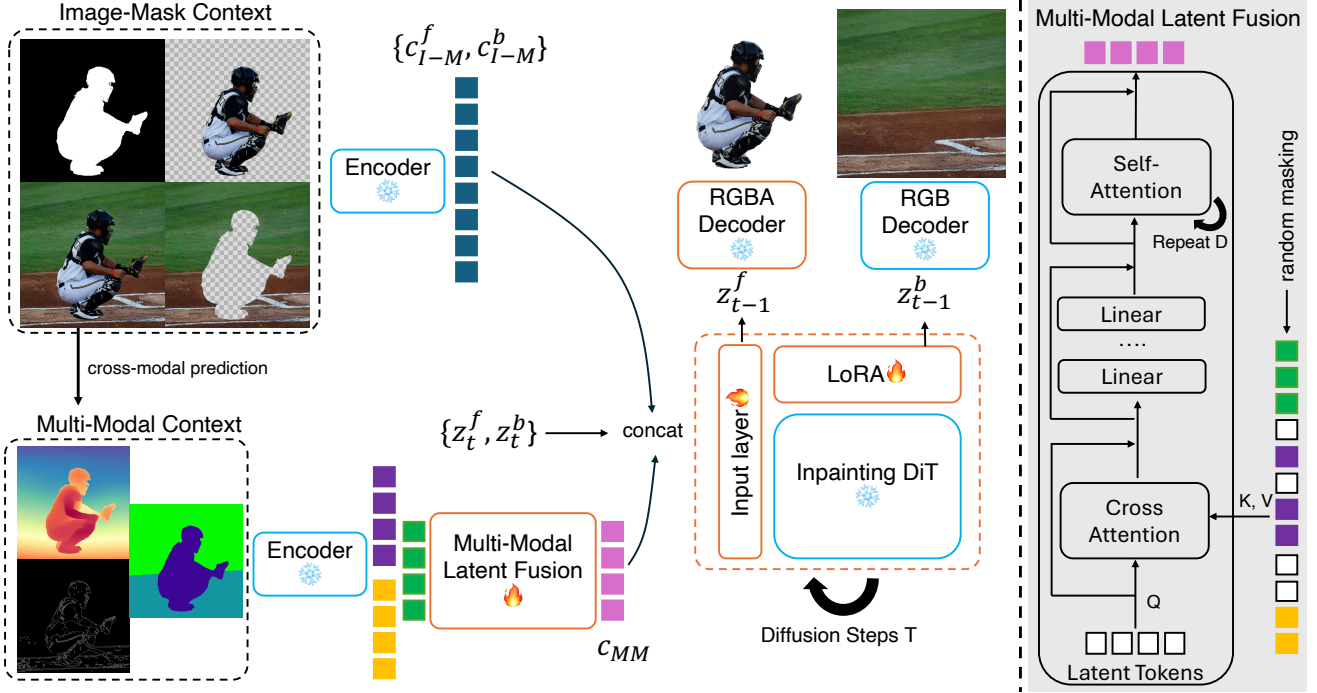


Figure 3. Detailed diagram of the key components in our proposed adaptation method. Light blue boxes denote components from the original pre-trained inpainting DiT model, while orange boxes represent our modifications or additions. Our approach efficiently incorporates both Image-Mask Context and Multi-Modal Context tokens to guide generation. After adaptation, the model can simultaneously output an extracted and outpainted foreground along with a clean, object-removed background.

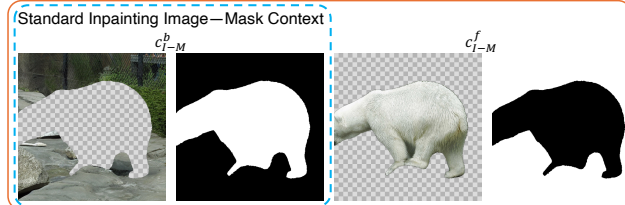


Figure 4. We illustrate the difference between the standard image-mask context used in diffusion-based inpainting models, shown in the light blue box as c_{I-M}^b , and our proposed image-mask context for image layer decomposition, shown in the orange box as $\{c_{I-M}^f, c_{I-M}^b\}$.

additional foreground image-mask context c_{I-M}^f . This foreground context serves as a control signal that helps the model balance preservation of existing information and generation of new content, enabling faithful extraction and outpainting of foreground objects.

After obtaining all context tokens from different sources, foreground context $c_{I-M}^f \in \mathbb{R}^{N \times d1}$, background context $c_{I-M}^b \in \mathbb{R}^{N \times d1}$, and fused multi-modal context $c_{MM} \in \mathbb{R}^{N \times d2}$, we concatenate them with the corresponding noisy input tokens for foreground $z_t^f \in \mathbb{R}^{N \times d3}$ and background $z_t^b \in \mathbb{R}^{N \times d3}$. The concatenation is performed along the channel dimension as follows: Foreground input: $\text{concat}(z_t^f, c_{I-M}^f, c_{MM}) \in \mathbb{R}^{N \times (d1+d2+d3)}$, Back-

ground input: $\text{concat}(z_t^b, c_{I-M}^b, c_{MM}) \in \mathbb{R}^{N \times (d1+d2+d3)}$. The final input to the DiT consists of two separate sequences of N tokens, one for the foreground and one for the background, each with a token dimension of $d1 + d2 + d3$.

3.5. Parameter Efficient Finetuning Protocol

Inspired by prior work, we adopt a similar Parameter-Efficient Fine-Tuning (PEFT) protocol to adapt the frozen base inpainting DiT for our task. This allows the model to handle additional input channels and learn new capabilities efficiently with few training iterations. Specifically, we finetune the input projection layer and insert LoRA (Low-Rank Adaptation) layers into each attention and feed-forward layer of the DiT backbone.

Notably, as demonstrated in our ablation study (Section 4.4.4), the LoRA rank plays a critical role in the detail preservation of foreground generation. It governs the trade-off between maintaining the generative power of the base inpainting model and learning the new capacity for foreground extraction, with the base model weights frozen.

3.6. Decoding Foreground and Background

The generated background is in RGB format, allowing us to directly reuse the pre-trained VAE encoder and decoder without modification. In contrast, the generated foreground is in RGBA format, which includes an additional alpha chan-

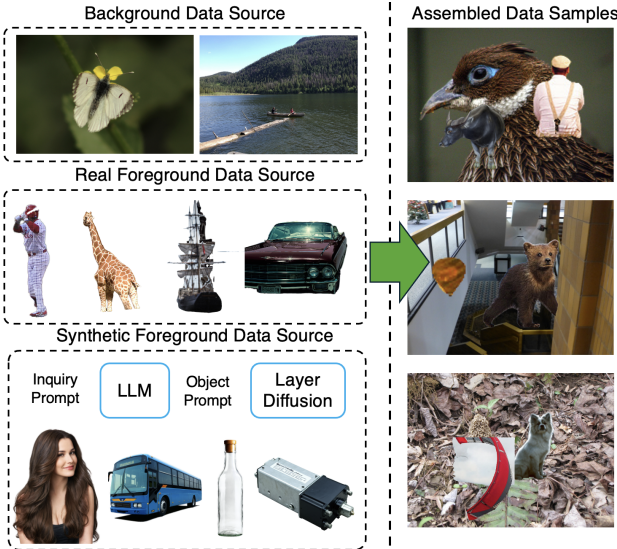


Figure 5. Our training data consists three sources: backgrounds, real foregrounds, and synthetic foregrounds.

nel for transparency. To support this, we finetune a separate RGBA encoder/decoder, following the same principles as prior works [34].

3.7. Training Data Curation from Public Sources

In this section, we explain how we curate our synthetic training dataset using public sources and tools. Our dataset includes key compositional elements commonly found in images, such as human, animals, objects, and indoor/outdoor scenes.

We use the MULAN [25] dataset, a real-world layered image dataset, as one of the foundation for RGBA foreground layers. However, as shown in Figure 5, images in MULAN often suffer from imperfect foreground extraction due to occlusions and background entanglement. To address this, we explore a text-to-layer generative model LayerDiffuse [34] to generate cleaner foregrounds. While these models produce complete foreground object shapes, they tend to introduce over-smoothed textures and lack fine details, leading to degraded training performance.

To harness the strengths of both sources of images, we propose a hybrid data strategy that combines two complementary foreground sources: 1) Real foregrounds with rich detail but incomplete shapes, 2) Generated foregrounds with complete shapes but limited texture fidelity. By merging these two types, we construct a more balanced and effective training dataset.

4. Experimental Results

4.1. Datasets and Implementation Details

For the base inpainting model, we adopt FLUX.1-Fill-dev [16] as the pre-trained diffusion transformer (DiT)¹. The default LoRA rank for training is 256. The input resolution is 1024x1024. The edge map is produced by Canny [3], the segmentation map is from SegFormer [28], and the depth map is from Depth-Anything-V2 [31]. We trained the model using standard flow matching loss with batch size 8, learning rate $5e-5$ for 7200 iterations. Our curated training data is constructed entirely from public datasets and tools, ensuring both accessibility and reproducibility. Layered image datasets based on real images are extremely limited. To the best of our knowledge, MULAN [25] is the only standard dataset in this domain. For foreground objects, we use real-world layered image from MULAN, as the primary source. We incorporate generated foreground layers from LayerDiffuse [34], guided by foreground prompts generated via ChatGPT-4o. We include examples of such prompts in the Supplementary Material. For background images, we sample from OpenImages [14], which are then overlaid by rescaled foregrounds to simulate realistic composite scenes. Each training image contains 1–3 foreground objects with possible occlusions. We intentionally use imperfect masks for training so the model learns to infer the accurate object boundary even in the cases of inaccurate input masks. In total, we assemble 100,000 image–foreground–background triplets, constructed entirely from public sources.

4.2. Evaluation Strategy

We compare our method against several state-of-the-art (SOTA) object removal baselines, including SD-XL Inpainting [5], PowerPoint [36], and our base pre-trained model, FLUX.1-Fill-dev. Quantitative evaluations are conducted on the 526 images from test sets of MULAN. Additionally, we perform qualitative comparisons on a diverse set of real-world images across various subjects and application domains to assess the quality of decomposed layers.

For evaluation, we employ standard metrics widely used in image reconstruction and object removal tasks, including PSNR, SSIM [26], LPIPS [35] and FID [8]. To further validate the practical effectiveness of our method, we also include results from a user study on the foreground generation quality, reflecting subjective human preferences and alignment with real-world use cases.

4.3. Qualitative and Quantitative Results

We report quantitative results on the MULAN test set to demonstrate the effectiveness of our method compared with baselines, as shown in Table 1. The metrics are computed

¹We use it only for research purpose and abide by their Non-Commercial License.

Method	PSNR \uparrow	SSIM \uparrow	LPIPS \uparrow	FID \downarrow
SDI	20.92	0.84	0.17	69.93
PowerPaint	23.46	0.76	0.17	41.67
FLux-I	25.59	0.92	0.09	35.96
Ours	27.30	0.93	0.08	25.97

Table 1. Quantitative metric comparison on the MULAN test set.

Method	Matting-Anything	DiffMatte	Ours
User Preference Rate	8.15%	32.34%	59.51%

Table 2. We performed a user study to compare the foreground generated with two matting baselines. The evaluation was carried out on our collected set of diverse real-world test images, allowing us to assess the practical effectiveness and visual quality of each method from the perspective of professional end users.

on background layers. Our adapted model achieves the best performance across all evaluation metrics, confirming the effectiveness of our approach. Furthermore, when compared to our base FLUX.1-Fill-dev model, our adaptation yields substantial improvements in background object removal, with a gain of 1.71 dB in PSNR and a reduction of 9.99 in FID.

To better evaluate our model’s performance, and to fairly compare against baselines for the foreground layers on real-world images, we collect 40 diverse high-quality real-world images. Since there is no open-source methods dedicated to layer decomposition, we compare with two matting methods that produce RGBA foregrounds, MattingAnything [17] and DiffMatte [10]. We conducted a user study with 18 independent researchers to assess the fidelity of the extracted foreground layers. We present the results of user study in Table 2. We also include some examples of qualitative comparison results in the Figure 6, image editing examples in Figure 7 and more in the supplementary materials.

4.4. Ablation Study

To evaluate the effectiveness of our design in adapting a pre-trained image inpainting diffusion model for the image layer decomposition task, we conduct a comprehensive ablation study. This analysis underscores the contribution of each design component, demonstrating their roles in balancing generative capability with faithful preservation of input details and contextual information.

4.4.1. The Impact of Base Model

To investigate the relationship between image inpainting and layer decomposition, we compare two base model choices: a pre-trained inpainting model (FLUX.1-Fill-dev) and a general image-to-image model (FLUX.1-Kontext-dev). As shown in Table 3, switching to the FLUX.1-Kontext-dev

Method	PSNR \uparrow	SSIM \uparrow	LPIPS \uparrow	FID \downarrow
r_{128}	26.34	0.92	0.09	33.92
r_{1024}	27.15	0.92	0.09	27.32
-w/o c_{I-M}^f	27.04	0.92	0.08	27.49
-w/o c_{MM}	27.16	0.93	0.08	28.02
kontext	26.22	0.92	0.09	36.14
Ours	27.30	0.93	0.08	25.97

Table 3. Quantitative metric comparison on object removal task to evaluate the effectiveness of our design. -w/o c_{I-M}^f : removes the foreground image-mask context. r_{128} and r_{1024} refer to LoRA ranks of 128 and 1024, respectively, used in parameter-efficient fine-tuning. -w/o c_{MM} : removes the multi-modal context component.

backbone leads to a performance drop, supporting our hypothesis that layer decomposition is best approached as an adaptation of the inpainting task.

4.4.2. The Impact of Image-Mask Context

As shown in Figure 8, the image-mask context plays a crucial role in our model by distinguishing between regions intended for generation and those meant for preservation. This allows the model to effectively control hallucinations arising from the inherent tension between completing missing content and faithfully retaining input details.

We also conduct a quantitative ablation study to evaluate the impact of our carefully designed image-mask context, as illustrated in Figure 4. Specifically, we compare our full context design, using both foreground and background image-mask context $\{c_{I-M}^f, c_{I-M}^b\}$, with the standard background-only image-mask context c_{I-M}^b typically used in inpainting tasks. The results of this comparison are reported in Table 3. When the foreground image-mask context c_{I-M}^f , is removed, we observe a drop of 0.26 dB in PSNR on the object removal task. More importantly, as shown in Figure 9, the model’s ability to faithfully extract foreground objects degrades significantly, beginning to hallucinate or alter content within the extracted regions. These findings validate the motivation behind our combined foreground-background image-mask context design: the inclusion of c_{I-M}^f plays a crucial role in mitigating hallucination and ensuring the faithful preservation of object regions during layer decomposition.

4.4.3. The Impact of Multi-modal Context

We present both quantitative and qualitative evaluations to assess the impact of multi-modal context on background object removal performance. As shown in Table 3, incorporating multi-modal context leads to a measurable improvement in quantitative metrics for the object removal task.

More noticeably, Figure 10 demonstrates that the inclusion of multi-modal cues, such as depth, segmentation, and

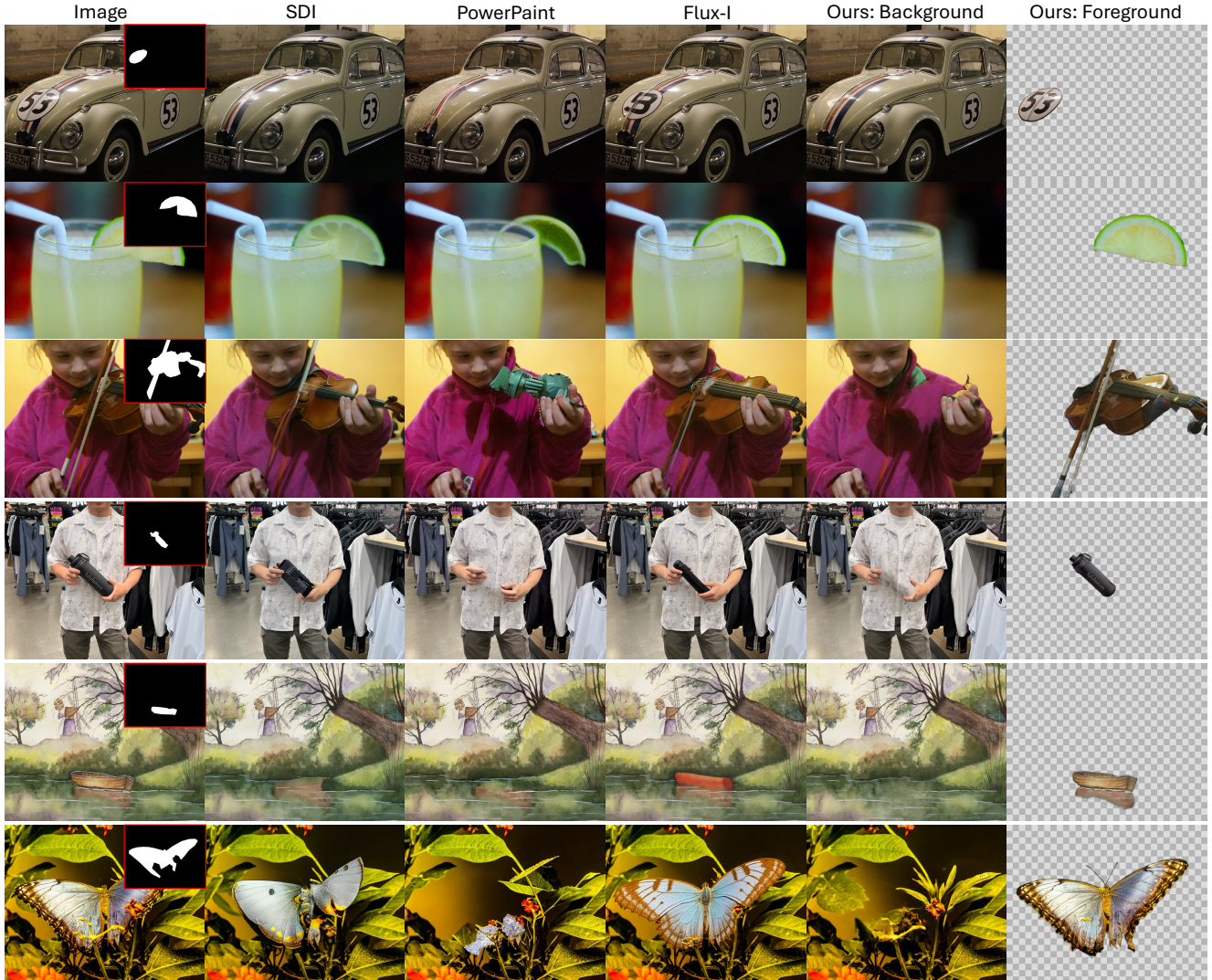


Figure 6. We present examples comparing our method against baselines on our collected real-world image test set for the object removal task. These qualitative results highlight the visual differences in foreground removal accuracy, background reconstruction quality, and consistency across various challenging scenes. Please zoom in for the best viewing quality.



Figure 7. Image editing examples. Layer decomposition enables manipulation of elements. Left: the original image, right: the edited image.

edge maps, helps the model better understand the semantics of the fill-in regions. This results in more accurate and visually consistent reconstructions. In contrast, without such context, the model is prone to hallucinations, often introducing unrealistic artifacts or structure in the removed regions. These results highlight the importance of multi-modal guid-

ance in reducing hallucination and improving background realism after object removal.

4.4.4. The Impact of LoRA Rank

As a general trade-off in LoRA-based Parameter-Efficient Fine-Tuning (PEFT) frameworks, the choice of LoRA rank

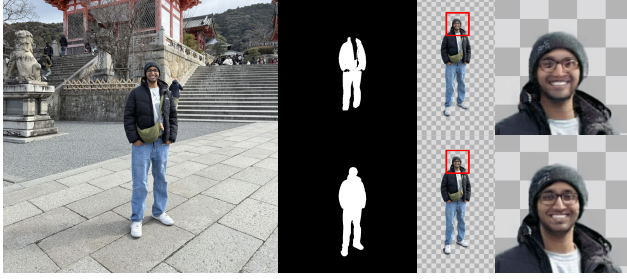


Figure 8. In this figure, we compare two foreground layer generation results from the same input image using different masks. The top row uses an incomplete mask that excludes the human head region, while the bottom row uses a nearly complete mask that includes it. We observe that when the head region is omitted, the model tends to hallucinate or modify that area. In contrast, with the complete mask, the model preserves the original head region, demonstrating its ability to balance generative filling and faithful content extraction based on the input mask.



Figure 9. Comparison of Ablation Models Using Different Image-Mask Contexts for Image Layer Decomposition. We compare models trained with the standard inpainting-only context c_{I-M}^b and our proposed dual-context design $\{c_{I-M}^f, c_{I-M}^b\}$. In (a), the foreground output is generated using only c_{I-M}^b , in (b), the foreground is generated using the combined context. The key difference is in content fidelity, model (a) tends to hallucinate or alter parts of the foreground, while model (b) better preserves the original object, demonstrating the importance of our dual-context design for faithful layer decomposition.

plays a crucial role. This trade-off is especially significant in our case due to two key factors: 1) Our base model is a pre-trained image inpainting diffusion model, originally trained for a different task. Adapting it to the novel task of image layer decomposition requires learning new capabilities while preserving its existing generative priors. 2) Our training data is entirely curated from public datasets and tools, which is inferior compared to the commercial-grade datasets used for training the original model. Together, these factors motivate a careful investigation into how the LoRA rank impacts the adaptation process, seeking an optimal trade-off between



Figure 10. Comparison of Object Removal with and without Multi-Modal Context. In this figure, we compare object removal performance under two conditions: (a) without multi-modal context, and (b) with multi-modal context. On the left side, we show the input image, mask, and the multi-modal context cues, which include depth maps, segmentation masks, and edge maps. On the right, we present the corresponding object removal outputs. The results clearly demonstrate that incorporating multi-modal context significantly improves object removal performance. The additional cues provide the model with richer spatial and semantic understanding of the scene, effectively reducing hallucinations and enhancing consistency and realism in the reconstructed areas.

preserving pre-trained priors and enabling the learning of new functionality. We report the quantitative ablation results in Table 3. As shown: a smaller rank 128 is insufficient for the model to fully learn the new task of layer decomposition. A larger rank 1024 enables greater adaptation but overwrites pre-trained priors, leading to hallucinations and sub-optimal performance. Based on these findings, we select a LoRA rank of 256 for our final model configuration, achieving the best balance between adaptability and stability.

5. Limitations and Future Work

As shown in the Supplementary Material, our method fails on some complex images including cluttered objects, large occlusions, and objects held in fingers. We attribute it to the lack of such intricate samples in the synthetic training dataset, and believe it will be alleviated with better training data in the future work.

6. Conclusion

In this paper, we demonstrate that image layer decomposition shares intrinsic similarities with in/outpainting. Leveraging this insight, we show that unlike prior works, our approach can achieve generative layer decomposition using only publicly available data, a lightweight adaptation of an inpainting model, and carefully designed modules to preserve context and reduce hallucinations. Our method achieves state-of-the-art performance with significantly lower data and computational requirements.

References

[1] Tomer Amit, Tal Shahrbany, Eliya Nachmani, and Lior Wolf. Segdiff: Image segmentation with diffusion probabilistic models. *arXiv preprint arXiv:2112.00390*, 2021. 2

[2] Stephen Batifol, Andreas Blattmann, Frederic Boesel, Saksham Consul, Cyril Diagne, Tim Dockhorn, Jack English, Zion English, Patrick Esser, Sumith Kulal, et al. Flux. 1 kontext: Flow matching for in-context image generation and editing in latent space. *arXiv e-prints*, pages arXiv–2506, 2025. 2

[3] John Canny. A computational approach to edge detection. *IEEE Transactions on pattern analysis and machine intelligence*, (6):679–698, 2009. 5

[4] Ciprian Corneanu, Raghudeep Gadde, and Aleix M Martinez. Latentpaint: Image inpainting in latent space with diffusion models. In *Proceedings of the IEEE/CVF winter conference on applications of computer vision*, pages 4334–4343, 2024. 2

[5] diffusers. stable-diffusion-xl-1.0-inpainting-0.1. <https://huggingface.co/diffusers/stable-diffusion-xl-1.0-inpainting-0.1>, 2023. 2, 5

[6] Sicheng Gao, Xuhui Liu, Bohan Zeng, Sheng Xu, Yanjing Li, Xiaoyan Luo, Jianzhuang Liu, Xiantong Zhen, and Baochang Zhang. Implicit diffusion models for continuous super-resolution. In *Proceedings of the IEEE/CVF conference on computer vision and pattern recognition*, pages 10021–10030, 2023. 2

[7] Ian J Goodfellow, Jean Pouget-Abadie, Mehdi Mirza, Bing Xu, David Warde-Farley, Sherjil Ozair, Aaron Courville, and Yoshua Bengio. Generative adversarial nets. *Advances in neural information processing systems*, 27, 2014. 2

[8] Martin Heusel, Hubert Ramsauer, Thomas Unterthiner, Bernhard Nessler, and Sepp Hochreiter. Gans trained by a two time-scale update rule converge to a local nash equilibrium. *Advances in neural information processing systems*, 30, 2017. 5

[9] Jonathan Ho, Ajay Jain, and Pieter Abbeel. Denoising diffusion probabilistic models. *Advances in neural information processing systems*, 33:6840–6851, 2020. 2

[10] Yihan Hu, Yiheng Lin, Wei Wang, Yao Zhao, Yunchao Wei, and Humphrey Shi. Diffusion for natural image matting. In *European Conference on Computer Vision*, pages 181–199. Springer, 2024. 2, 6

[11] Andrew Jaegle, Felix Gimeno, Andy Brock, Oriol Vinyals, Andrew Zisserman, and Joao Carreira. Perceiver: General perception with iterative attention. In *International conference on machine learning*, pages 4651–4664. PMLR, 2021. 3

[12] kandinsky community. Kandinsky 2.2. <https://huggingface.co/kandinsky-community/kandinsky-2-2-decoder-inpaint>, 2023. 2

[13] Diederik P Kingma and Max Welling. Auto-encoding variational bayes. *arXiv preprint arXiv:1312.6114*, 2013. 2

[14] Alina Kuznetsova, Hassan Rom, Neil Alldrin, Jasper Uijlings, Ivan Krasin, Jordi Pont-Tuset, Shahab Kamali, Stefan Popov, Matteo Malloci, Alexander Kolesnikov, et al. The open images dataset v4: Unified image classification, object detection, and visual relationship detection at scale. *International journal of computer vision*, 128(7):1956–1981, 2020. 5

[15] Gihyun Kwon and Jong Chul Ye. Diffusion-based image translation using disentangled style and content representation. *arXiv preprint arXiv:2209.15264*, 2022. 2

[16] Black Forest Labs. Flux. <https://github.com/black-forest-labs/flux>, 2025. 2, 5

[17] Jiachen Li, Jitesh Jain, and Humphrey Shi. Matting anything. In *Proceedings of the IEEE/CVF Conference on Computer Vision and Pattern Recognition*, pages 1775–1785, 2024. 6

[18] Andreas Lugmayr, Martin Danelljan, Andres Romero, Fisher Yu, Radu Timofte, and Luc Van Gool. Repaint: Inpainting using denoising diffusion probabilistic models. In *Proceedings of the IEEE/CVF conference on computer vision and pattern recognition*, pages 11461–11471, 2022. 1, 2

[19] Kangfu Mei, Hossein Talebi, Mojtaba Ardakani, Vishal M Patel, Peyman Milanfar, and Mauricio Delbracio. The power of context: How multimodality improves image super-resolution. In *Proceedings of the Computer Vision and Pattern Recognition Conference*, pages 23141–23152, 2025. 3

[20] Fabio Quattrini, Vittorio Pippi, Silvia Cascianelli, and Rita Cucchiara. Alfie: Democratising rgba image generation with no. In *European Conference on Computer Vision*, pages 38–55. Springer, 2024. 2

[21] Robin Rombach, Andreas Blattmann, Dominik Lorenz, Patrick Esser, and Björn Ommer. High-resolution image synthesis with latent diffusion models. In *Proceedings of the IEEE/CVF conference on computer vision and pattern recognition*, pages 10684–10695, 2022. 2

[22] Shuyao Shang, Zhengyang Shan, Guangxing Liu, LunQian Wang, XingHua Wang, Zekai Zhang, and Jinglin Zhang. Resdiff: Combining cnn and diffusion model for image super-resolution. In *Proceedings of the AAAI Conference on Artificial Intelligence*, pages 8975–8983, 2024. 1

[23] Roman Suvorov, Elizaveta Logacheva, Anton Mashikhin, Anastasia Remizova, Arsenii Ashukha, Aleksei Silvestrov, Naejin Kong, Harshith Goka, Kiwoong Park, and Victor Lempitsky. Resolution-robust large mask inpainting with fourier convolutions. In *Proceedings of the IEEE/CVF winter conference on applications of computer vision*, pages 2149–2159, 2022. 2

[24] Keyu Tian, Yi Jiang, Zehuan Yuan, Bingyue Peng, and Liwei Wang. Visual autoregressive modeling: Scalable image generation via next-scale prediction. *Advances in neural information processing systems*, 37:84839–84865, 2024. 2

[25] Petru-Daniel Tudor, Yongxin Yang, Shifeng Zhang, Fei Chen, Steven McDonagh, Gerasimos Lampouras, Ignacio Iacobacci, and Sarah Parisot. Mulan: A multi layer annotated dataset for controllable text-to-image generation. In *Proceedings of the IEEE/CVF Conference on Computer Vision and Pattern Recognition*, pages 22413–22422, 2024. 2, 5

[26] Zhou Wang, Alan C Bovik, Hamid R Sheikh, and Eero P Simoncelli. Image quality assessment: from error visibility to structural similarity. *IEEE transactions on image processing*, 13(4):600–612, 2004. 5

[27] Bin Xia, Yulun Zhang, Shiyin Wang, Yitong Wang, Xinglong Wu, Yapeng Tian, Wenming Yang, Radu Timofte, and Luc

Van Gool. Diffi2i: Efficient diffusion model for image-to-image translation. *IEEE Transactions on Pattern Analysis and Machine Intelligence*, 2024. [1](#)

[28] Enze Xie, Wenhui Wang, Zhiding Yu, Anima Anandkumar, Jose M Alvarez, and Ping Luo. Segformer: Simple and efficient design for semantic segmentation with transformers. *Advances in neural information processing systems*, 34:12077–12090, 2021. [5](#)

[29] Shaoan Xie, Zhifei Zhang, Zhe Lin, Tobias Hinz, and Kun Zhang. Smartbrush: Text and shape guided object inpainting with diffusion model. In *Proceedings of the IEEE/CVF conference on computer vision and pattern recognition*, pages 22428–22437, 2023. [2](#)

[30] Jinrui Yang, Qing Liu, Yijun Li, Soo Ye Kim, Daniil Pakhomov, Mengwei Ren, Jianming Zhang, Zhe Lin, Cihang Xie, and Yuyin Zhou. Generative image layer decomposition with visual effects. In *Proceedings of the Computer Vision and Pattern Recognition Conference*, pages 7643–7653, 2025. [1](#), [2](#)

[31] Lihe Yang, Bingyi Kang, Zilong Huang, Zhen Zhao, Xiaogang Xu, Jiashi Feng, and Hengshuang Zhao. Depth anything v2. *Advances in Neural Information Processing Systems*, 37: 21875–21911, 2024. [5](#)

[32] Jiahui Yu, Zhe Lin, Jimei Yang, Xiaohui Shen, Xin Lu, and Thomas S Huang. Generative image inpainting with contextual attention. In *Proceedings of the IEEE conference on computer vision and pattern recognition*, pages 5505–5514, 2018. [2](#)

[33] Tao Yu, Zongyu Guo, Xin Jin, Shilin Wu, Zhibo Chen, Weiping Li, Zhizheng Zhang, and Sen Liu. Region normalization for image inpainting. In *Proceedings of the AAAI conference on artificial intelligence*, pages 12733–12740, 2020. [2](#)

[34] Lvmin Zhang and Maneesh Agrawala. Transparent image layer diffusion using latent transparency. *arXiv preprint arXiv:2402.17113*, 2024. [2](#), [5](#)

[35] Richard Zhang, Phillip Isola, Alexei A Efros, Eli Shechtman, and Oliver Wang. The unreasonable effectiveness of deep features as a perceptual metric. In *Proceedings of the IEEE conference on computer vision and pattern recognition*, pages 586–595, 2018. [5](#)

[36] Junhao Zhuang, Yanhong Zeng, Wenran Liu, Chun Yuan, and Kai Chen. A task is worth one word: Learning with task prompts for high-quality versatile image inpainting. In *European Conference on Computer Vision*, pages 195–211. Springer, 2024. [5](#)

From Inpainting to Layer Decomposition: Repurposing Generative Inpainting Models for Image Layer Decomposition

Supplementary Material

7. Example prompts for generating foreground materials with LayerDiffuse

performance can be further enhanced with better training data covering these challenging cases.

animal	common object	complex object	machine	human
dog	apple	coral	microwave	tall man
cat	banana	brain	refrigerator	slim man
cow	robot	pinecone	freezer	young woman
...
profession	household	clothes	sci-fi objects	traffic objects
businessman	sofa	shirt	laser gun	car
policeman	armchair	pants	plasma rifle	truck
fireman	loveseat	shorts	ion blaster	motorcycle
...

Table 4. Prompt categories and examples used to generate foreground object layers with LayerDiffuse.

In our data curation process, we use LayerDiffuse to generate synthetic foreground layers. Prompts are categorized into major themes, with ChatGPT-4o generating examples for each. We collected around 300 prompts per category. Sample prompts are shown in Table 4.

8. More Qualitative Examples

In Figure 11, we present examples in the user study where our foreground layers are compared against two matting methods: Matting-Anything and DiffMatte. Our method is superior in preserving the detail shapes and recovering occlusions.

In Figure 12, we present more examples of object removal as the same setting in the main paper, with comparisons against SD-XL Inpainting, PowerPaint and Flux.1-Fill-dev.

9. Effectiveness of Pre-trained VAE Encoding for Multi-Modal Inputs

In Figure 13, we visually confirm that the pre-trained VAE of the FLUX model can effectively encode and decode edge maps, segmentation maps, and depth maps, modalities used in our multi-modal context input, without noticeable detail loss. This validates our design choice of using the pre-trained VAE to tokenize these modalities efficiently.

10. Failure Cases

We show examples of failure cases in Figure 14. Our method has challenges in complex cases involving cluttered objects, large objects or hand-object interaction. We believe the

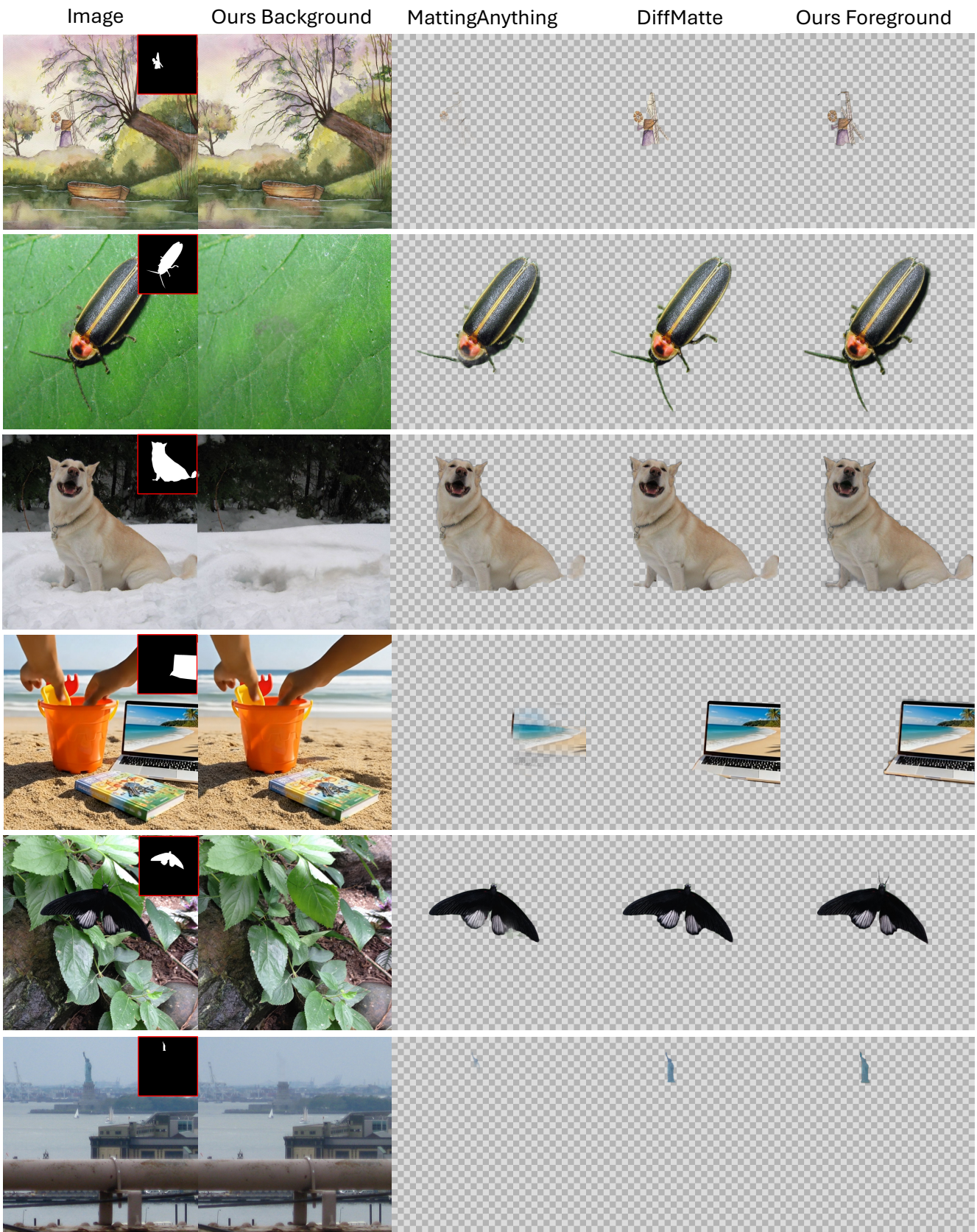


Figure 11. We present additional comparisons of foreground extraction using two matting methods, Matting-Anything and DiffMatte, both of which produce RGBA foreground layers.

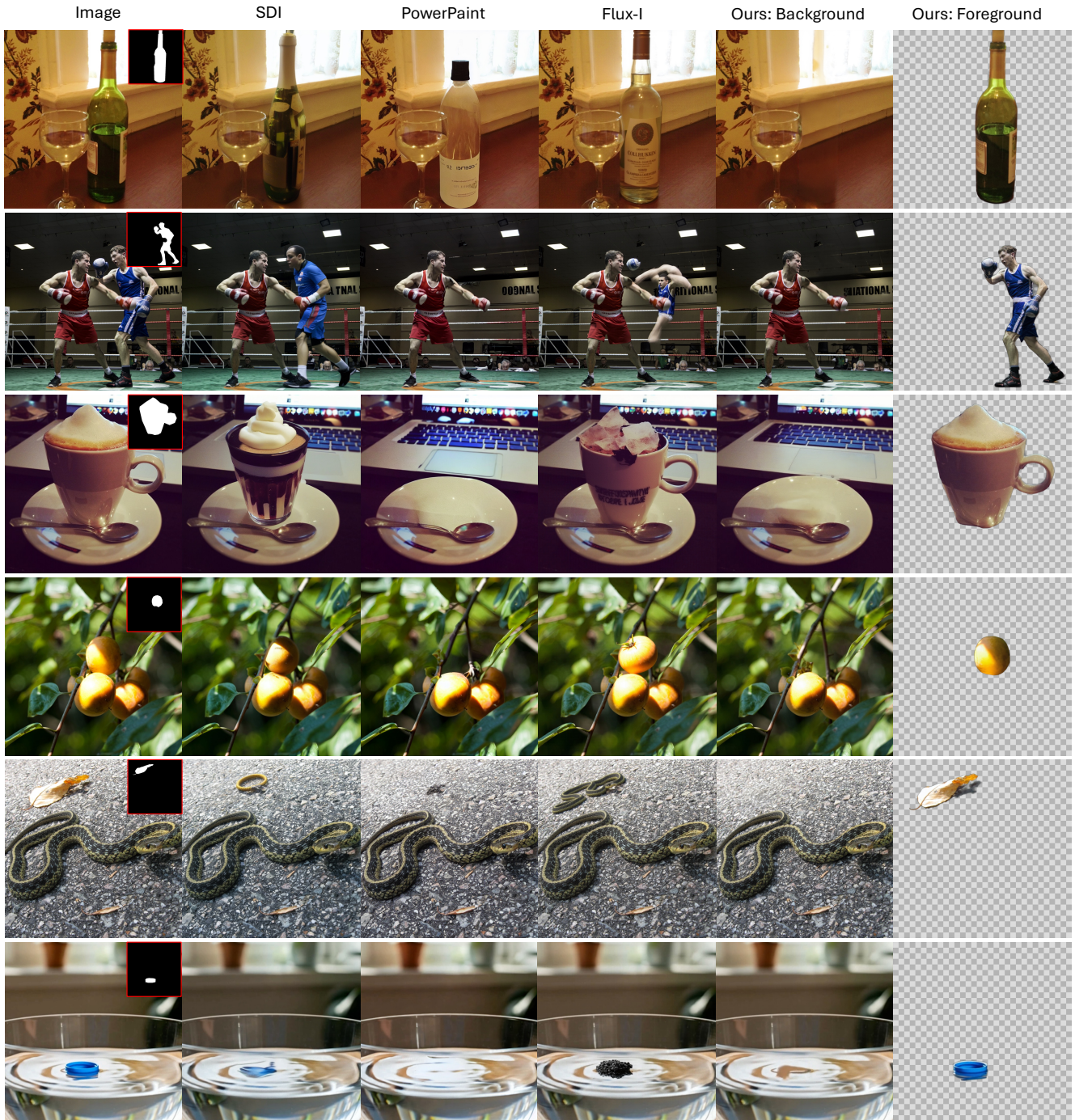


Figure 12. We present additional comparisons of object removal as the same setting in the main paper.

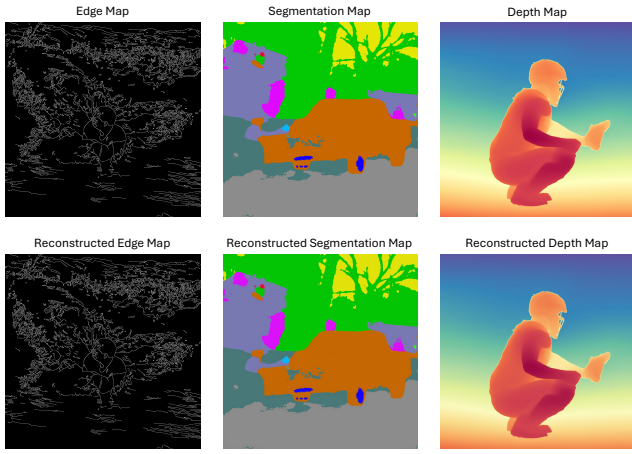


Figure 13. Visual results showing the pre-trained FLUX VAE’s ability to reconstruct various modalities, edge map, segmentation map, and depth map, used in our multi-modal context.



Figure 14. We show examples of failure cases. The model tends to fail on complex images that involve cluttered objects, large objects with occlusion, and hand-object interaction.